Optical image recognition of underwater bubbles

Zhang Hao, Li Xiangchun, Yang Qian, Wu Chengxuan, Lei Zhuo

(1. Institute of Oceanographic Instrumentation, Qilu University of Technology (Shandong Academy of Sciences), Qingdao 266061, China;
2. Shandong Provincial Key Laboratory of Ocean Environmental Monitoring Technology, Qingdao 266061, China)

Abstract: A new method of bubble recognition using optical underwater imaging was presented by employing Zernike moments and gray gradient, to differentiate bubbles from solid particles. This method included 3 parts: image division, image pre-processing and feature extraction for bubble recognition. Firstly, images of the suspended particles were obtained from underwater particle database, in which a particular bubble was divided and selected manually from the whole. Secondly, image pre-processing was employed to enhance single bubble images, to extract and represent bubble silhouette and gray level. Thus, the database of bubble features were selected and formed. Finally, the shape descriptor, Zernike moments, was utilized to measure the similarity with features of other suspended particles to differentiate circle particles from the irregular ones. Subsequently, the center of circle particle and the trend of gray gradient were computed, so as to distinguish the bubbles from solid particles. The experimental results show that, the accuracy of bubble recognition is up to 94%. It is concluded that this method not only recognizes bubbles from irregular suspensions, but also improves gray gradients calculation for enhanced results. By extracting and distinguishing object features through the prospects of both shape and gray, this method enhances the accuracy of bubble recognition, with higher precision and broader suitability.

Key words: underwater optical imaging; bubble recognition; Zernike moments; gradient computation
CLC number: TP391.4 **Document code:** A **DOI:** 10.3788/IRLA201948.0326001

水下气泡光学图像识别方法

张 浩,李向春,杨 倩,吴承璇,雷 卓

(1. 齐鲁工业大学(山东省科学院) 山东省科学院海洋仪器仪表研究所,山东 青岛 266061;
2. 山东省海洋环境监测技术重点实验室,山东 青岛 266061)

摘 要: 针对水中气泡与固体悬浮微粒不易区分的问题,提出了一种基于 Zernike 矩与灰度计算的水下光学气泡图像识别方法。该方法主要分为图像划分、图像预处理和特征提取三个步骤。首先,获取水下悬浮微粒的图像,从中划分出单个气泡并选取部分样本;为了更好地提取与表示气泡轮廓与灰度特征,然后采用图像预处理方法增强气泡边缘特征,选择并构建气泡特征库;最后,采用 Zernike 矩计算悬浮微粒特征的相似度,区分圆形微粒与非圆形微粒,之后计算微粒中心与灰度变化趋势,辨别气泡与固体悬浮微粒。实验结果表明,在测试数据集上的气泡识别准确率达到 94%。该方法不仅能够辨

收稿日期: 2018-10-05; **修订日期:** 2018-11-03
基金项目: 国家自然科学基金(41206165);山东省科学院基础研究基金(2018-11);山东省重大科技创新工程项目(2018YFJH0705)
作者简介: 张浩(1980-),男, 博士,主要从事水下光学成像与计算机视觉方面的研究。Email:haozhang2013@126.com

别圆形与非圆形微粒,而且能够融合灰度梯度计算方法以获取更好的结果。该方法从形状与灰度两个方面提取与辨别目标的特征信息,提高了气泡识别精度,具有较高的精确性与适用性。

关键词:水下光学成像; 气泡识别; Zernike 矩; 梯度计算

0 Introduction

As suspended particles are key underwater matters, they can influence the quality of water and underwater ecology, such as phytoplankton and zooplankton. Bubbles are mixed in suspended particles, and they play an important role in underwater ambience similarly.

Bubbles are important to many processes of interest in geophysics[1-3], as well as in other disciplines such as chemical engineering[4], biopharmaceuticals[5], and wastewater management[6], among many others. Within geophysics, bubble plumes from breaking waves are either dominant or very important to processes as diverse as air-sea gas transfer[7], marine aerosol formation[8-11], surface micro-layer enrichment[12], ship wake bubbles[13], and 3D measurement in optical microscopy[14]. Each of these processes has potentially important impacts on both global and regional scales.

Bubbles both directly and indirectly enhance atmosphere-ocean exchange of gases that are important to global climate, such as methane, carbon dioxide, and fluorocarbons. Bubbles directly exchange entrained atmospheric gas with the ocean by diffusion of the gas through the bubble-ocean interface. Indirectly they contribute to gas exchange by disrupting the surface microlayer[15], by generating turbulence as they rise in the upper ocean[13], and by the release of entrained gas when they burst at the surface [7]. Additionally, bubble plume formation (i.e., wave breaking) is inextricably linked with turbulence generation. These turbulence formation mechanisms alter the turbulent velocity profile within the oceanic boundary layer, thereby enhancing gas transfer [15]. Bubble plumes also cause bulk fluid motions, such as an upwelling flow[16], enhancing mixing and gas transfer.

Due to their importance, the development of bubble measurement systems (BMSs) to determine the bubble size distribution (number of bubbles per unit volume per size increment) has long interested researchers. Cao et al employed self-made simple lighting bubble instrument according to optical theory and took photographs of underwater bubbles[17]. Leifer et al designed an in-site instrument for underwater bubbles, proposed an optical measurement by photograph[18], and presented a method of bubble images calibration[19]. Having employed this instrument, Leifer et al measured the bubble size and concentration[20]. In optical BMS, bubble recognition is an important method in distinguishing bubbles and particles. Therefore, we employ Zernike moments and gray gradient to implement the differentiation of the bubbles from underwater particles, to improve bubble concentration and size in computation subsequently.

1 Zernike moment

Zernike moments are defined in terms of a set of orthogonal functions with simple rotation properties known as Zernike polynomials[21-23]. These polynomials were originally introduced by Zernike in 1934 and are widely used in the analysis of optical systems. They form a complete orthogonal set of complex polynomials over the interior of the unit circle. This orthogonality condition makes the polar coordinate system more suitable to express these functions.

The definition of Zernike moment[24] is as follow:

$$Z_{pq}=\frac{p+1}{\pi}\int_0^{2\pi}\int_0^1 V_{pq}^*(r,\theta)f(r,\theta)r\mathrm{d}r\mathrm{d}\theta,\ r\leqslant 1 \qquad (1)$$

where, $f(r,\theta)$ is an image which is expressed in polar coordinates. Then p is non-negative integer, i.e. $p=0,1,2,\cdots,\infty$. And q is positive integer subject to the constraints, $p-q$ is even and $p\geqslant q$. The symbol "*" denotes conjugate complex number. $V_{pq}(r,\theta)$ is Zernike polynomials as below:

$$V_{pq}(r,\theta)=R_{pq}(r)e^{jq\theta} \tag{2}$$

where, $R_{pq}(r)$ is the radial polynomials defined as:

$$R_{pq}(r)=\sum_{k=0}^{(p-|q|)/2}\frac{(-1)^k(p-k)!}{k!\left(\frac{p+|q|}{2}-k\right)!\left(\frac{p-|q|}{2}-k\right)!}r^{p-2k} \tag{3}$$

Zernike polynomials are orthogonal in a circle as follow:

$$\int_0^{2\pi}\int_0^1 V_{nl}^*(r,\theta)V_{mk}(r,\theta)r\mathrm{d}r\mathrm{d}\theta=\frac{\pi}{n+1}\delta_{nm}\delta_{lk} \tag{4}$$

There is a discrete image $f(x,y)$ with $N\times N$ pixels, and its Zernike moments are defined as

$$Z_{pq}=\frac{p+1}{\pi(N-1)^2}\sum_{x=1}^{N}\sum_{y=1}^{N}V_{pq}^*(r,\theta)f(x,y) \tag{5}$$

where, $r=\sqrt{(x^2+y^2)}/N$, $\theta=\arctan(y/x)$.

Zernike moment and geometric moment can be expressed in following equation:

$$Z_{pq}=\frac{p+1}{\pi}\sum_{s=q}^{p}\sum_{l=0}^{(s+q)/2}\sum_{m=0}^{(s-q)/2}(-1)^j(j)^{l+m}\binom{\frac{s+q}{2}}{l}\binom{\frac{s-q}{2}}{m}B_{pqs}\mu_{s-l-m,l+m} \tag{6}$$

where,

$$B_{pqk}=\frac{(-1)^{(p-k)/2}((p+k)/2)!}{((p-k)/2)!\ ((k+q)/2)!\ ((k-q)/2)!} \tag{7}$$

We can reconstruct the function of image, $f(x,y)$, by the finite number of Zernike moments as follow:

$$f(r,\theta)\cong\sum_{p=0}^{n}\sum_{q}Z_{pq}V_{pq}(r,\theta) \tag{8}$$

Zernike moments are employed in pattern recognition widely, as its amplitude is good at rotational invariance.

We employ $f(r,\theta+\alpha)$ to denote the image rotated α, so the Zernike moments of $f(r,\theta+\alpha)$ is expressed as:

$$Z_{pq}'=\frac{p+1}{\pi}\iint f(r,\theta)[V_{pq}(r,\theta+\alpha)]^*r\mathrm{d}r\mathrm{d}\theta=Z_{pq}\exp(-jq\alpha) \tag{9}$$

As it is $||Z_{pq}||=||Z_{pq}'||$ and the symbol $||\cdot||$ denotes normal number, the amplitudes of Zernike moments are invariant.

An eigenvector of any sample, u, is in n dimensions, so that the eigenvectors in the samples span an eigenspace in n dimensions. Consequently, the Euclidean distance $||u-v||$ between the acquiring image u and the model image v represents their similarities, and both u and v are respectively represented by $n-$order invariant moments of their own. So their distance between the object and the model in invariant moments is defined as:

$$d(u,v)=||u-v||=||v-u||=\sqrt{\sum_{i=1}^{n}(u_i-v_i)^2}=\sqrt{\sum_{i=1}^{n}(Z_{iq}^0-Z_{iq}^1)^2} \tag{10}$$

Here, Z_{iq}^0 and Z_{iq}^1 represent $n-$order invariant moments of the acquiring image and the model image respectively. The less the differences between u and v are, the more similar both images are. Otherwise, the more the differences are, the less similar. We normalize the similarity of invariant moment, that is, calculating the similarity between each acquiring images and the model, so we define the similar function as in Eq. (11).

$$\alpha=1-\frac{d(u,v)}{\max(d(u,v))} \tag{11}$$

Here, $\alpha\in[0,1]$ and the more α is, the more similar the acquiring image is, otherwise, the less similar.

2 Proposed method

As so many suspended particles are underwater, it is of great significance to differentiate bubbles from these particles. Having obtained bubble images previously, we presented a method to distinguish the bubbles from the others, such as particles.

As to recognize underwater bubbles from particles by shapes and gray gradient, our method has 3 key steps: image division, image pre-procession and feature extraction, bubble recognition, as shown in Fig.1. In the first step, we obtain underwater bubble images from the image database, manually divide the

single bubble from the image and select some bubble images from them. In the second step, we employ methods of image processing to handle single bubble images, and extract and represent feature of silhouette and gray from these images. In the last step, we utilize the shape descriptor, Zernike moments, to classify above features so as to differentiate shapes of suspended particles, and then compute bubble gray gradient in image edge to distinguish the bubbles and particles in similar shapes.

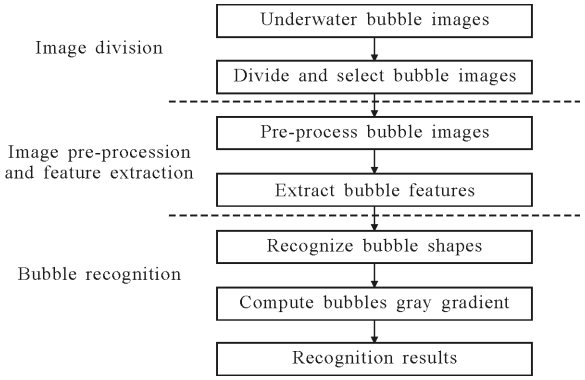

Fig.1 Procedure of bubble recognition

First, as shown in Fig.2, we conduct the bubble database by several steps below:

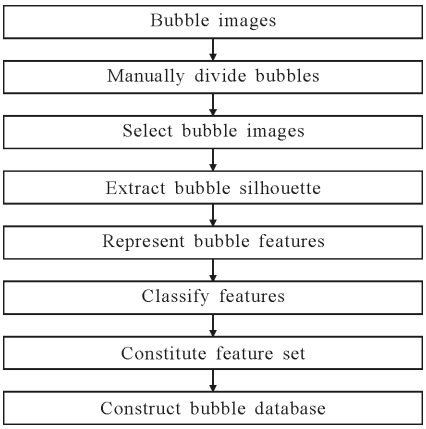

Fig.2 Construction of bubble database

(1) Input underwater images into this procedure; (2) Divide bubbles from the image one by one manually to form a set; (3) Select some bubbles from the set as key ones; (4) Extract bubble features of the silhouette; (5) Represent these features with vectors; (6) Employ Zernike moments to classify these features by shape into different groups; (7) Construct different classes from different groups so as to form a database of bubble shape.

Next, we implement the silhouette recognition of bubbles by ten steps in Fig.3.

(1) Acquire images of background underwater; (2) Employ Gaussian mixture model (GMM) to build dynamic background by several images; (3) Acquire images of underwater suspensions; (4) Extract subjects from background image by background subtraction; (5) Divide subjects from the background; (6) Extract silhouettes of suspended particles; (7) Represent subject features with vectors; (8) Measure the similarity between the features in the database and above; (9) Classify subjects above and put them into one category; (10) Obtain the results of bubbles.

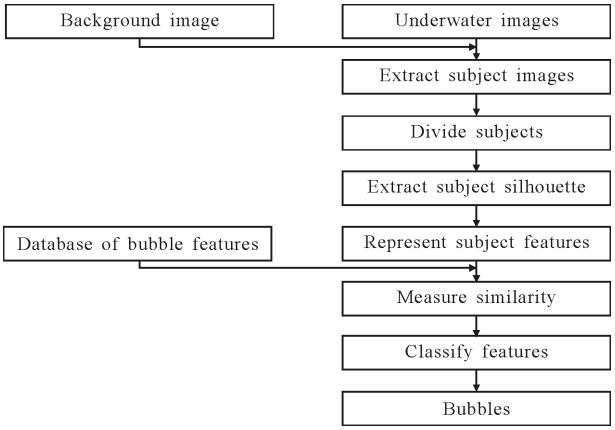

Fig.3 Procedure of bubble silhouette recognition

In the step(8) of Fig.3, we utilize Zernike moments to measure the similarity between the obtained ones and the model in the database as seen in Fig.4.

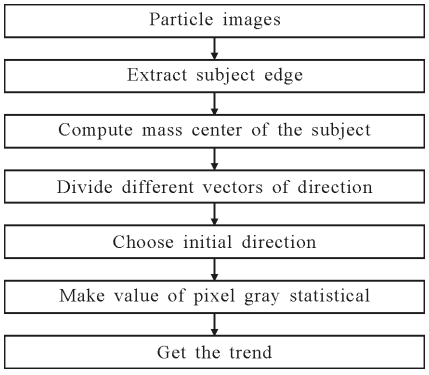

Fig.4 Flowchart of gray trend of bubble

(1) Extract the pixels in the verge of subjects;

(2) Compute the center of mass in the subject by

$$\begin{cases} x_c=\dfrac{1}{N_b}\sum_{i=1}^{N_b} x_i \\ y_c=\dfrac{1}{N_b}\sum_{i=1}^{N_b} y_i \end{cases} \tag{12}$$

Here, (x_c,y_c) represents the center of mass, N_b is the sum of pixel number on the subject verge, and (x_i,y_i) denotes the position of the pixel;

(3) Divide the circle into 8 different divisions evenly from the center, as shown in Fig.5;

(4) Choose the initial vector along x-axis, and then they are defined as P_0, P_1, …, P_7 counterclockwise;

(5) Make value of pixels gray statistical along each direction;

(6) Get the trend of pixels gray.

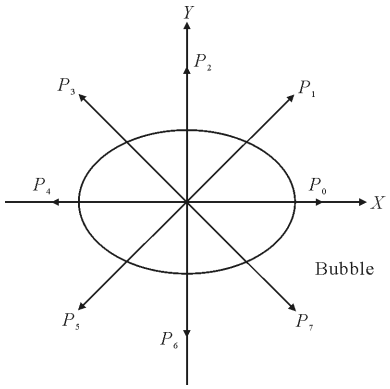

Fig.5 Directions of vectors

3 Experimental results and analysis

3.1 Experimental platform

To obtain images of suspended particles, we design an experimental platform for underwater particles by visual method, which chiefly includes a steel platform, a water tank, a module of light, a light shield, a diffusion screen, and a camera with lens.

There is a convex bed in the middle of the steel platform. On the bed, there is a water tank for monitoring underwater particles. On the bottom of the platform, there is a horizontal rail. On this rail, there are three sliders for holding the light, the light shield including diffusion screen, and the camera, as seen in Fig.6. The light and the camera are opposite on different sides of the diffusion screen.

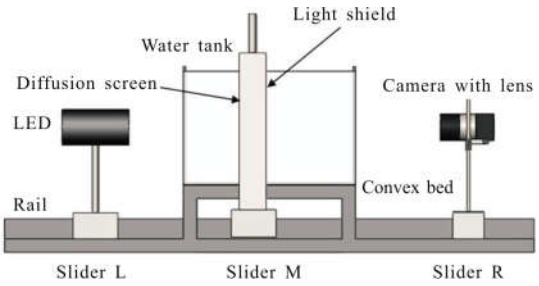

Fig.6 Experimental platform of underwater bubbles

Before experiment starts, we can adjust the view of the camera just opposite to the emitting orientation of light, so the camera can obtain the images of underwater particles when the light is on. In the experiment, the image of underwater particles is captured by the camera with high resolutions, as shown in Fig.7. When the suspended particles are dim in the camera, we can move Slider L, M and R to and fro, as it is essential to keep different ambience.

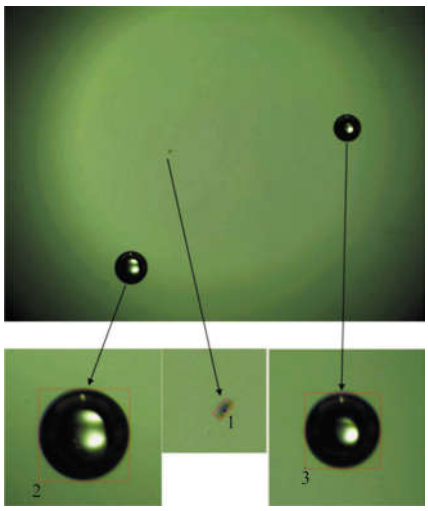

Fig.7 Samples of underwater bubbles

3.2 Experimental results

We implemented this method by above-mentioned platform of underwater sampling, and then obtained bubble images to form a feature set and subsequently construct the database. There is fresh water in the water tank, and we disturb it by air

pump so that we can obtain bubbles and suspended particles. The samples of underwater bubbles and solid particles are extracted and shown in Fig.8.

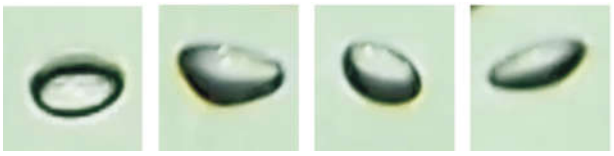

(a) Bubbles

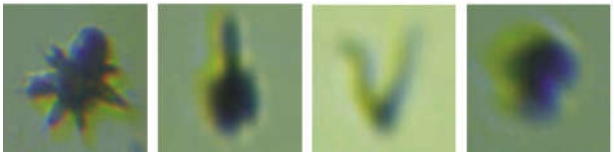

(b) Solid particles

Fig.8 Samples of underwater bubbles and solid particles

First, we selected 3 groups of samples from the database as training set, each of which includes 10 samples. We can employ the procedure of construction of the bubble database to form feature sets. Next, we selected another 10 groups of samples as testing set. Similarly, the authors proposed the method of bubble recognition based on normalized intensity in previous work[20]. Their accuracy of bubble recognition is approximate to 90%, as it only employs statistical gray. Our accuracy of bubble recognition is up to 94%, as it employs not only statistical gray but also Zernike moments. The accuracy of recognition is seen in Tab.1. We can conclude that the blurred images in Group 7 reduce recognition accuracy. Analyzing previous experimental results, we obtain that empirical value of α is 0.85. That is

$$R=\begin{cases}1 & \alpha\geqslant 0.85\\ 0 & \alpha<0.85\end{cases}$$

where R is the recognition result. If α is no less than 0.85, we denote it as success, otherwise, as failure.

Comparing both methods above, we can conclude that, the former one, which obtains 8 vectors in different directions, is more powerful; whereas the latter one only focuses horizontal value of bubbles gray. The latter one is less effective for the bubble whose light spot is not in the center.

Tab.1 Recognition results of the proposed method

Group ID	#1	#2	#3	#4	#5	Avg.
Accuracy	100%	100%	90%	100%	90%	–
Group ID	#6	#7	#8	#9	#10	94
Accuracy	100%	80%	100%	90%	90%	–

After recognition, we employ the algorithm of size reversal to compute equivalent particle diameter (EPD). We can conclude physical size of underwater particles from Fig.7, such as length, width, and the results are listed in Tab.2.

Tab.2 Reversal results of underwater particles in Fig.7

ID	Number of pixel		Reversal value/μm		
	Length	Width	Length	Width	EPD
#1	38	19	59.02	29.51	41.73
#2	291	287	451.95	445.74	448.83
#3	240	239	372.74	371.19	371.96

4 Conclusions

We introduced the visual experimental platform for underwater particles, which can capture the bubble images for training and testing. Then we proposed a new method for bubble recognition, including bubble modeling, bubble silhouette recognition and bubble differentiation. Finally, a better accuracy is obtained in 3 groups of samples for training and 10 groups for testing. The advantage of this method is that we employ less training samples to recognize more testing ones. The downside is that it is less effective for small bubbles in size, such as sizes of less than 10 pixel× 10 pixel. In the future, we plan to employ cameras with lens in higher resolutions for the small bubbles for more accuracy.

References:

[1] Farmer D M, McNeil C L, Johnson B D. Evidence for the

importance of bubbles in increasing air-sea gas flux [J]. ***Nature***, 1993, 361(18): 620-623.

[2] Asher W E, Karle L M, Higgins B J, et al. The influence of bubble plumes on air-seawater gas transfer velocities[J]. ***Journal of Geophysical Research***, 1996, 101(C5): 12027-12041.

[3] Woolf D K. Bubbles and Their Role in Gas Exchange[M]. Cambridge: Cambridge University Press, 1997: 174-205.

[4] Clift R, Grace J R, Weber M E. Bubbles, Drops, and Particles[M]. New York: Academic Press, 1978: 244-284.

[5] Kawase Y, Halard B, Moo-Young M. Liquid phase mass transfer coefficients in bioreactors [J]. ***Biotechnology and Bioengineering***, 1992, 39: 1133-1140.

[6] Asselin C, Comeau Y, Ton-That Q A. Alpha correction factors for static aerators and fine bubble diffusers used in municipal facultative aerated lagoons [J]. ***Water Science & Technology***, 1998, 38: 79-85.

[7] Liss P S, Watson A J, Bock E J, et al. Physical Processes in the Microlayer and the Air-sea Exchange of Trace Gases [M]. Cambridge: Cambridge University Press, 1997: 1-33.

[8] Blanchard D C. Electrification of the atmosphere by particles from bubbles in the sea [J]. ***Progress in Oceanography***, 1963, 1: 73-197.

[9] Monahan E C. The Ocean as a Source for Atmospheric Particles[M]. Berlin: Springer, 1986: 129-163.

[10] De Leeuw G. Spray droplet source function: From laboratory to open ocean [C]//Proceedings of a Workshop on Modeling the Fate and Influence of Marine Spray, 1990: 17-28.

[11] Spiel D E. On the births of film drops from bubbles bursting on seawater surfaces [J]. ***Journal of Geophysical Research***, 1998, 103(C11): 24907-24918.

[12] Blanchard D C. The ejection of drops from the sea and their enrichment with bacteria and other materials: A review [J]. ***Estuaries***, 1989, 12(3): 127-137.

[13] Tian Jing, Bai Guangfu, Jiang Yang. Research of scattering Stokes parameters for ship wake bubbles [J]. ***Infrared and Laser Engineering***, 2018, 47(2): 0206003. (in Chinese)

[14] Liu Jian, Gu Kang, Li Mengzhou, et al. 3D measurement decoupling criterion in optical microscopy [J]. ***Infrared and Laser Engineering***, 2017, 46(3): 0302001. (in Chinese)

[15] Kitaigorodskii S A, Donelan M A. Wind-wave effects on gas transfer[J]. Switzerland: Springer, 1984: 141-170.

[16] Asher W E, Karle L M, Higgins B J. On the difference between bubble-mediated air-water transfer in freshwater and seawater[J]. ***Journal of Marine Research***, 1997, 55(5): 1-34.

[17] Cao Ruixue. Measurement and analysis of bubbles in ocean surface layer and sub-surface layer[D]. Qingdao: Institute of Oceanology, Chinese Academy of Sciences, 2006. (in Chinese)

[18] Leifer I, MacDonald I. Dynamics of the gas flux from shallow gas hydrate deposits: Interaction between oily hydrate bubbles and the oceanic environment [J]. ***Earth and Planetary Science Letters***, 2003, 210: 411-424.

[19] Lifer I, De Leeuw G, Kunz G, et al. Calibrating optical bubble size by the displaced-mass method [J]. ***Chemical Engineering Science***, 2003, 58: 5211-5216.

[20] Leifer I, De Leeuw G, Cohen L H. Optical measurement of bubbles: System, design and application [J]. ***American Meteorological Society***, 2003, 20: 1317-1332.

[21] Bhatia A B, Wolf E. On the circle polynomial of Zernike and related orthogonal sets [J]. ***Mathematical Proceedings of the Cambridge Philosophical Society***, 1954, 50(1): 40-48.

[22] Teh C-H, Chin R T. On image analysis by the method of moments [J]. ***IEEE Transaction on Pattern Analysis and Machine Intelligence***, 1988, 10(4): 496-513.

[23] Teague M R. Image analysis via the general theory of moments [J]. ***Journal of the Optical Society of America***, 1980, 70(8): 920-930.

[24] Belkasim S, Hassan E, Obeidi T. Explicit invariance of Cartesian Zernike moments [J]. ***Pattern Recognition Letters***, 2007, 28: 1969-1980.